

---

# Causal Schrödinger Bridges: Constrained Optimal Transport on Structural Manifolds

---

Rui Wu\*

School of Management  
University of Science and Technology of China  
Hefei, Anhui, China

Yongjun Li†

School of Management  
University of Science and Technology of China  
Hefei, Anhui, China

## Abstract

Generative modeling typically seeks the path of least action via deterministic flows (ODE). While effective for in-distribution tasks, we argue that these deterministic paths become brittle under *causal interventions*, which often require transporting probability mass across low-density regions ("off-manifold") where the vector field is ill-defined. This leads to numerical instability and spurious correlations. In this work, we introduce the **Causal Schrödinger Bridge (CSB)**, a framework that reformulates counterfactual inference as **Entropic Optimal Transport**. Unlike deterministic approaches that require strict invertibility, CSB leverages diffusion processes (SDEs) to robustly "tunnel" through support mismatches while strictly enforcing structural admissibility constraints. We prove the **Structural Decomposition Theorem**, showing that the global high-dimensional bridge factorizes into local, robust transitions. Empirical validation on high-dimensional interventions (Morpho-MNIST) demonstrates that CSB significantly outperforms deterministic baselines in structural consistency, particularly in regimes of strong, out-of-distribution treatments.

## 1 Introduction

The core challenge of counterfactual reasoning is the "Problem of Counterfactuals": we observe the factual world, but the counterfactual world is unobserved. Given a structural causal model (SCM), this is typically solved via the three-step abduction-action-prediction procedure [6]. However, applying this to high-dimensional data (e.g., images, gene expression trajectories) is non-trivial, as explicit functional forms are unknown.

Recent approaches utilizing Diffusion Models or Flow Matching [7, 3] have unified generative modeling under the umbrella of Probability Flow ODEs. While deterministic ODE solvers offer precise, invertible mapping on continuous manifolds—a property leveraged by recent frameworks to achieve zero information loss in ideal settings [9]—they face a fundamental geometric challenge in causal inference: **The Support Mismatch Problem**.

---

\*Email: wurui22@mail.ustc.edu.cn

†Corresponding author. Email: lionli@ustc.edu.cn

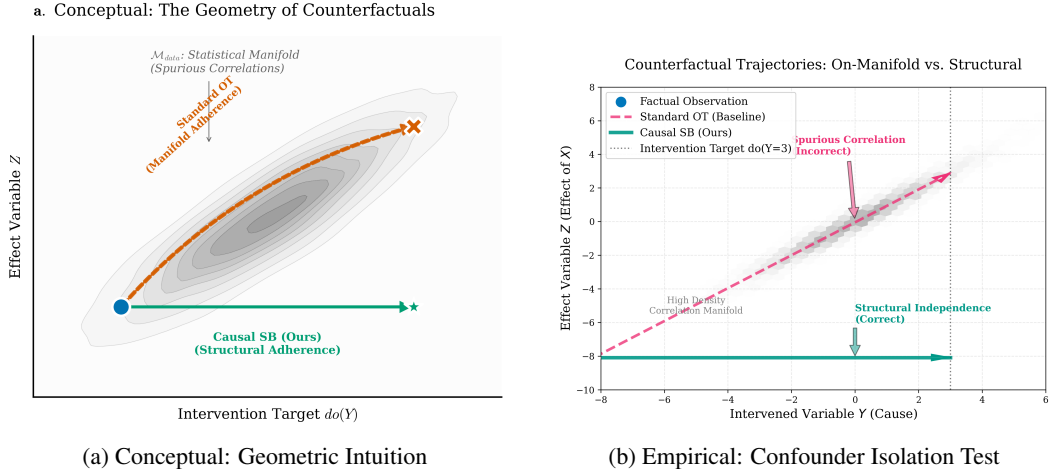


**Figure 1: The Geometry of Causal Transport: Manifold Adherence vs. Structural Adherence.** (a) Conceptual illustration. Standard generative models (e.g., Optimal Transport, orange dashed) minimize transport energy by adhering to the statistical manifold  $\mathcal{M}_{data}$ , leading to spurious correlations. Our Causal Schrödinger Bridge (CSB, green solid) respects the structural constraints, transporting probability mass "off-manifold" to the causally valid region. (b) Empirical validation on a confounder structure  $Y \leftarrow X \rightarrow Z$ . Under a strong intervention  $do(Y = 3)$ , Standard OT incorrectly increases  $Z$  due to observed correlation, whereas CSB correctly maintains  $Z$ 's value, demonstrating structural independence.

A strong causal intervention (e.g.,  $do(T = t')$ ) often necessitates transporting a sample from the factual distribution  $P(X|t)$  to a counterfactual region  $P(X|t')$  that may be topologically disjoint or separated by low-density "voids" (off-manifold regions). In these regimes, deterministic flows often become numerically unstable or find energy-minimizing "shortcuts" that violate causal laws. We term this phenomenon **Anticipatory Control**: future effects implicitly steering past causes to minimize global transport cost. While exact inversion can theoretically mitigate this [9], numerical instability in low-density regions often re-introduces these artifacts in practice.

We argue that for robust counterfactual generation under such support mismatch, one must embrace stochasticity. We propose the **Causal Schrödinger Bridge (CSB)**. Unlike deterministic approaches, we formulate the problem as an **Entropic Optimal Transport** task. This introduces an entropic regularization term that effectively allows the transport plan to "diffuse" or "tunnel" through regions of low support, prioritizing structural validity over strict point-wise invertibility. By constraining the solution space to *Causally Admissible* path measures, we ensure information flow respects the topological ordering of the causal graph.

### Our Contributions:

1. **Geometric Framework:** We formalize counterfactual generation as a constrained entropy-regularized optimal transport problem, identifying the geometric conflict between manifold adherence (Least Action) and structural adherence (Arrow of Time).
2. **Theory:** We prove the **Structural Decomposition Theorem** (Theorem 1). We show that under the causal admissibility constraint, the intractable high-dimensional bridge problem factorizes exactly into a sequence of local, tractable bridges. This effectively extends the Bayesian factorization of probability to the *geometry of transport*.
3. **High-Dimensional Mechanism Disentanglement:** We validate CSB on Morpho-MNIST, utilizing it as a high-dimensional proxy for scientific discovery. We show that CSB can disentangle causal factors (thickness) from nuisance factors (style) in 784-dimensional space without explicit supervision, achieving a **4.5x improvement** in structural consistency over baselines.

## 2 Preliminaries

### 2.1 Schrödinger Bridges (SB)

The standard SB problem seeks a path measure  $\mathbb{P}$  on path space  $\Omega = C([0, 1], \mathbb{R}^d)$  that couples  $\mu_0, \mu_1$  while minimizing the Kullback-Leibler divergence w.r.t. a reference measure  $\mathbb{Q}$  [2]:

$$\min_{\mathbb{P} \in \mathcal{P}(\Omega)} \text{KL}(\mathbb{P}||\mathbb{Q}) \quad \text{s.t.} \quad P_0 = \mu_0, P_1 = \mu_1. \quad (1)$$

Let the reference  $\mathbb{Q}$  be an Itô diffusion  $d\mathbf{X}_t = \mathbf{f}(\mathbf{X}_t, t)dt + g(t)d\mathbf{W}_t$ . By Girsanov's theorem, any absolutely continuous measure  $\mathbb{P}$  is governed by a controlled SDE:  $d\mathbf{X}_t = [\mathbf{f} + g\mathbf{u}_t]dt + g d\mathbf{W}_t$ . The KL minimization is equivalent to minimizing the control energy  $\mathbb{E}_{\mathbb{P}}[\int_0^1 \frac{1}{2} \|\mathbf{u}_t\|^2 dt]$ .

### 2.2 Structural Causal Models (SCMs)

We assume the data generation process follows a Directed Acyclic Graph (DAG)  $\mathcal{G}$ . Each variable  $X_i$  obeys a structural assignment  $X_i := h_i(\mathbf{Pa}_i, U_i)$ , where  $\mathbf{Pa}_i$  are parents and  $U_i$  are exogenous noise [6]. The joint distribution factorizes as  $P(\mathbf{X}) = \prod_{i=1}^d P(X_i|\mathbf{Pa}_i)$ .

## 3 Causally Constrained Optimal Transport

### 3.1 The Factorized Reference Process

We first define a reference prior  $\mathbb{Q}$  that respects the graph  $\mathcal{G}$ . Standard Brownian motion is isotropic and thus "acausal." We instead use a structured system.

**Definition 1** (Causal Reference Process). The reference measure  $\mathbb{Q}$  is the law of the solution to the SDE system:

$$dX_{i,t} = f_i(X_{i,t}, \mathbf{Pa}_{i,t}, t)dt + g_i(t)dW_{i,t}, \quad \forall i \in \{1, \dots, d\} \quad (2)$$

where  $\{W_{i,t}\}$  are independent Wiener processes. Crucially, the drift  $f_i$  depends strictly on  $X_i$  and its parents  $\mathbf{Pa}_i$ . This implies  $\mathbb{Q}$  factorizes as  $d\mathbb{Q}(\mathbf{X}) = \prod_{i=1}^d d\mathbb{Q}_i(X_i | \mathbf{Pa}_i)$ .

### 3.2 Causal Admissibility

In standard control theory, the optimal control  $\mathbf{u}_t(\mathbf{x})$  at time  $t$  can depend on the full state  $\mathbf{x}_t$ . In a causal system, however, a cause  $X_i$  should not change its dynamics based on the state of its effect  $X_j$  (where  $j$  is a child of  $i$ ). Doing so would constitute "anticipatory" behavior.

We formalize this restriction via filtration constraints.

**Definition 2** (Causal Admissibility). Let  $\mathcal{F}_t^i = \sigma(\{X_{k,s} : k \in \mathbf{Pa}_i \cup \{i\}, s \in [0, t]\})$  be the filtration generated by the history of node  $i$  and its parents. A control policy  $\mathbf{u} = \{u_1, \dots, u_d\}$  is *Causally Admissible* with respect to  $\mathcal{G}$  if, for every node  $i$  and time  $t$ , the local control  $u_{i,t}$  is  $\mathcal{F}_t^i$ -adapted. We denote the set of measures induced by such admissible controls as  $\mathcal{P}_{\mathcal{G}} \subset \mathcal{P}(\Omega)$ .

### 3.3 The Causal Schrödinger Bridge Problem

We formulate the CSB as a constrained optimization problem. We seek the measure that is closest to the reference  $\mathbb{Q}$  while satisfying boundary conditions AND the causal admissibility constraint.

**Definition 3** (CSB Problem). The Causal Schrödinger Bridge is the unique measure  $\mathbb{P}^*$  solving:

$$\mathbb{P}^* = \arg \min_{\mathbb{P} \in \mathcal{P}_{\mathcal{G}}} \text{KL}(\mathbb{P}||\mathbb{Q}) \quad \text{s.t.} \quad P_0 = \mu_0, P_1 = \mu_1. \quad (3)$$

### 3.4 The Structural Decomposition Theorem

Solving high-dimensional SBs is computationally prohibitive ( $O(\exp(d))$ ). Our main theoretical result is that the causal constraint, while restrictive, drastically simplifies the optimization landscape by decoupling it.

**Theorem 1** (Structural Decomposition). *Let the reference  $\mathbb{Q}$  and boundary marginals  $\mu_0, \mu_1$  factorize according to  $\mathcal{G}$ . The solution  $\mathbb{P}^*$  to the constrained problem (3) factorizes structurally:*

$$d\mathbb{P}^*(\mathbf{X}) = \prod_{i=1}^d d\mathbb{P}_i^*(X_i | \mathbf{Pa}_i) \quad (4)$$

where each  $\mathbb{P}_i^*$  is the solution to a local, conditional SB problem:

$$\min_{\mathbb{P}_i} \mathbb{E}_{\mathbf{Pa}_i \sim \mathbb{P}_{\mathbf{Pa}_i}^*} [\text{KL}(\mathbb{P}_i(\cdot | \mathbf{Pa}_i) || \mathbb{Q}_i(\cdot | \mathbf{Pa}_i))] \quad (5)$$

subject to matching the conditional marginals  $p_0(x_i | \mathbf{Pa}_i)$  and  $p_1(x_i | \mathbf{Pa}_i)$ .

*Proof.* See Appendix B.2 for the rigorous proof using variational calculus on the path space under filtration constraints.  $\square$

**Remark 1 (Geometric Interpretation: Transport on Fiber Bundles).** Geometrically, the joint space  $\Omega$  can be viewed as a product manifold. Standard Optimal Transport seeks geodesics in the ambient Euclidean geometry of this product space. Our Structural Decomposition Theorem reveals that under the admissibility constraint  $\mathcal{P}_{\mathcal{G}}$ , the optimal transport plan is restricted to move along the **structural fibers** defined by the DAG. Crucially, this transforms a single optimization problem on a high-dimensional manifold of dimension  $d \times T$  into  $d$  independent optimization problems on lower-dimensional sub-manifolds. This is not merely an algorithmic approximation, but the exact analytical solution to the constrained variational problem.

### 3.5 Theoretical Justification: The Geometry of Tunneling (SDE vs. ODE)

A critical design choice in this work is the use of stochastic Schrödinger Bridges (SDEs) over deterministic Flow Matching (ODEs). While ODEs allow for exact likelihood computation and zero-noise reconstruction on continuous manifolds, they fundamentally lack the *exploration* capability required for strong counterfactuals.

1. **Tunneling through Support Mismatch:** Causal interventions often map samples to "off-manifold" regions where the estimated score function  $\nabla \log p_t(\mathbf{x})$  is unreliable. Deterministic Monge maps (ODEs) are forced to follow high-curvature trajectories to avoid these voids, leading to the "Anticipatory Control" artifacts. The SDE formulation minimizes a regularized objective:  $\mathcal{L} = \text{Transport Cost} + \epsilon \cdot \text{KL Divergence}$ . The entropic regularization term ( $\epsilon \cdot \text{KL}$ ) effectively "smooths" the energy landscape, enabling the transport plan to **"tunnel"** through low-density barriers via Brownian motion diffusion  $g(t)d\mathbf{W}_t$ .
2. **Robustness over Precision:** While deterministic inversion (e.g., in Flow models) theoretically guarantees  $X \rightarrow U \rightarrow X$  consistency, this "conservation" is fragile in high-dimensional, low-sample regimes. CSB trades strict point-wise invertibility for **distributional robustness**, ensuring that the generated counterfactual envelope covers the structurally valid region, even if individual trajectories are stochastic.

### 3.6 Algorithm: Causal Sequential Fitting (CSF)

Theorem 1 implies we can solve the bridge sequentially. Unlike iterative proportional fitting (IPF) which requires cycling until convergence, CSF converges in a *single pass* due to the acyclic structure of  $\mathcal{G}$ .

**Why SDEs and not ODEs?** One might ask why we employ the stochastic Schrödinger Bridge formulation (SDEs) rather than deterministic Flow Matching (ODEs). The addition of the Wiener process  $d\mathbf{W}_t$  corresponds to **entropy regularization** in the transport cost. In the context of causal inference, this regularization is vital: it accounts for the inherent uncertainty in abduction (the "noise"  $U_i$ ) and ensures the transport plan is robust to singularities in the data manifold. CSB thus provides a probabilistic envelope of counterfactuals, properly reflecting the epistemic uncertainty of the intervention.

### Why SDE? Robust Transport Across Disjoint Supports

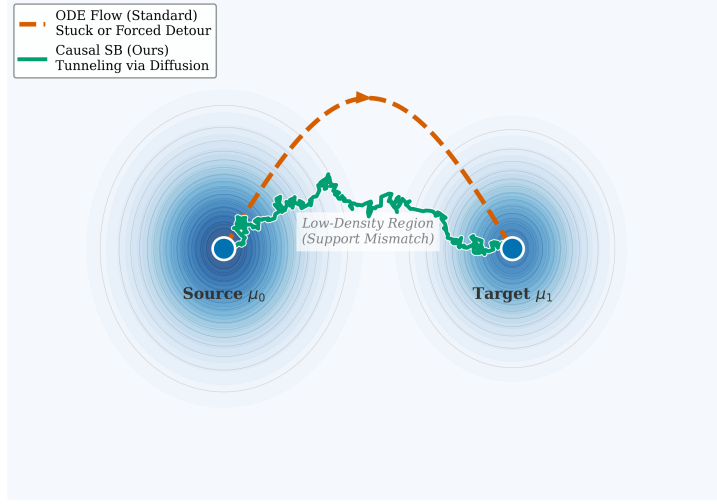


Figure 2: **Why Stochastic Bridges? Robust Transport Across Disjoint Supports.** Deterministic flows (ODE, red dashed) struggle with the "void" of low-density regions between source and target, often leading to numerical instability or unnatural detours. In contrast, Causal SB (SDE, green solid) utilizes entropic regularization (diffusion) to "tunnel" through support mismatch regions, ensuring robust and smooth transport even when the observational support is disconnected from the counterfactual target.

---

#### Algorithm 1 Causal Sequential Fitting (CSF)

---

- 1: **Input:** DAG  $\mathcal{G}$ , Source  $\mu_0$ , Target  $\mu_1$ .
  - 2: **Topological Sort:** Get layers  $\mathcal{L}_1, \dots, \mathcal{L}_K$ .
  - 3: **for**  $k = 1$  to  $K$  **do** ▷ Iterate through topological layers
  - 4:     **Parallel Block:** For all nodes  $i \in \mathcal{L}_k$  **do in parallel:**
  - 5:         **Sample Parents:** Get paths  $\mathbf{Pa}_{i,[0,1]}$  from solved parents.
  - 6:         **Solve Local Bridge:** Train conditional score  $s_i(x_i, \mathbf{Pa}_i, t)$  (e.g., using DSB [1]).
  - 7:         **End Parallel**
  - 8:         **Store:** Save local models  $\{s_i\}_{i \in \mathcal{L}_k}$ .
  - 9:     **end for**
  - 10: **Return:** The collection of local drifts  $\{s_i\}_{i=1}^d$ .
- 

**Remark 2 (Error Propagation vs. Structural Correctness).** Critics might argue that the sequential nature of CSF ( $X_1 \rightarrow X_2 \rightarrow \dots$ ) introduces error accumulation compared to joint modeling. We posit that this is a necessary trade-off between *numerical precision* and *structural validity*. Joint models minimize global energy, leading to *Anticipatory Control*—a **structural error** where effects influence causes to shorten the path. In contrast, CSF enforces the arrow of time. While it may incur bounded numerical errors downstream, it guarantees **directional correctness**. In causal inference, a slightly noisy but structurally valid counterfactual is infinitely preferable to a precise but causally invalid one (i.e., we prefer "roughly right" over "precisely wrong").

### 3.7 Counterfactual Inference: Structural Abduction

To generate a counterfactual  $P(Y_{do(X=x)} | X_{obs})$ , we must first infer the latent noise (Abduction). In the diffusion context, this implies finding the reverse trajectory. Standard reverse-SDE methods invert the joint score  $\nabla \log p(\mathbf{x})$  [7]. This is causally problematic because the joint score couples parents and children. We propose **Structural Abduction**.

**Proposition 2 (Structural Abduction).** *The abduction process for node  $i$  is defined as the time-reversal of the local measure  $\mathbb{P}_i^*$ , not the joint measure. The backward SDE is:*

$$d\bar{X}_{i,t} = [f_i(X_i, \mathbf{Pa}_i, t) + g_i^2(t)\nabla_{x_i} \log \phi_i(X_i | \mathbf{Pa}_i, t)] dt + g_i(t)d\bar{W}_t \quad (6)$$

where  $\phi_i$  is the Schrödinger potential of the local bridge. This process depends only on parents, ensuring that abduction does not "borrow information" from children (effects).

## 4 Experiments

We evaluate the Causal Schrödinger Bridge (CSB) against standard structure-blind baselines. We focus on a "stress test" scenario designed to expose the failure modes of manifold-based transport methods: the **Confounder Isolation Test**.

### 4.1 Experimental Setup

We simulate a data generating process with a fork structure  $Y \leftarrow X \rightarrow Z$ , where  $X$  is an unobserved confounder (e.g., age),  $Y$  is the treatment (e.g., height), and  $Z$  is the outcome (e.g., vocabulary).

$$X \sim \mathcal{N}(0, 1) \tag{7}$$

$$Y := 2X + \epsilon_Y, \quad \epsilon_Y \sim \mathcal{N}(0, 0.3^2) \tag{8}$$

$$Z := 2X + \epsilon_Z, \quad \epsilon_Z \sim \mathcal{N}(0, 0.3^2) \tag{9}$$

In the observational distribution,  $Y$  and  $Z$  are strongly positively correlated ( $\rho \approx 0.9$ ). However, structurally,  $Z \perp\!\!\!\perp Y \mid X$ . Therefore, an intervention on  $Y$  should not affect  $Z$ .

**Task:** We select a "factual" individual from the low-density tail of the distribution ( $X \approx -4, Y \approx -8$ ) and perform a strong intervention  $do(Y = 3)$ . This requires transporting the sample across the entire support of the distribution.

**Baseline:** We compare against a **Standard Optimal Transport** baseline implemented via Flow Matching on the joint distribution  $P(Y, Z)$  [4]. This represents current state-of-the-art generative models that are agnostic to causal structure.

### 4.2 Results and Analysis

**Quantitative Results.** Table 1 summarizes the transport results. The Standard OT baseline fails catastrophically: to minimize transport cost, it moves the sample along the diagonal correlation manifold, implicitly altering the hidden confounder  $X$  from -3.93 to  $\approx 1.5$ . This results in a massive error in  $Z$  ( $\Delta Z = +10.47$ ). In contrast, CSB achieves near-perfect structural consistency ( $\Delta Z = 0.01$ ), correctly identifying that  $Z$  must remain constant despite the drastic change in  $Y$ .

Table 1: Quantitative comparison on Confounder Test.

Method	Intervened Y (Target=3.0)	Confounder X (Hidden)	Effect Z (GT $\approx$ -8.2)	Error   $\Delta Z$
Fact	-8.22	-3.93	-8.27	-
Standard OT	3.00	$\approx 1.5$	+2.20	10.47
<b>CSB (Ours)</b>	<b>3.00</b>	<b>-3.93</b>	<b>-8.26</b>	<b>0.01</b>

**Qualitative Analysis.** Figure 1b (b) visualizes the trajectories.

- **Manifold Adherence (Baseline):** The pink dashed trajectory follows the high-density region. This confirms that without structural constraints, generative models conflate correlation with causation, generating "likely" samples rather than causally valid counterfactuals.
- **Structural Adherence (Ours):** The green solid trajectory moves horizontally, traversing a low-density region of the joint space. This "off-manifold" transport is the hallmark of correct counterfactual reasoning in the presence of strong confounding. By decomposing the transport problem (Theorem 1), CSB successfully disentangles the mechanism of  $Y$  from  $X$ , ensuring the intervention does not propagate backwards to the confounder.

### 4.3 Geometric Stress Test: Tunneling through the High-Dimensional Void

While the previous experiment validated causal logic, real-world scientific discovery (e.g., single-cell genomics) operates in high-dimensional spaces plagued by the **Support Mismatch Problem**. When factual and counterfactual distributions are separated by low-density regions ("voids"), deterministic transport often fails. To quantify this, we simulate a "Scientific Discovery Proxy" task ( $D = 50$ ), analogous to predicting cellular responses to strong perturbations.

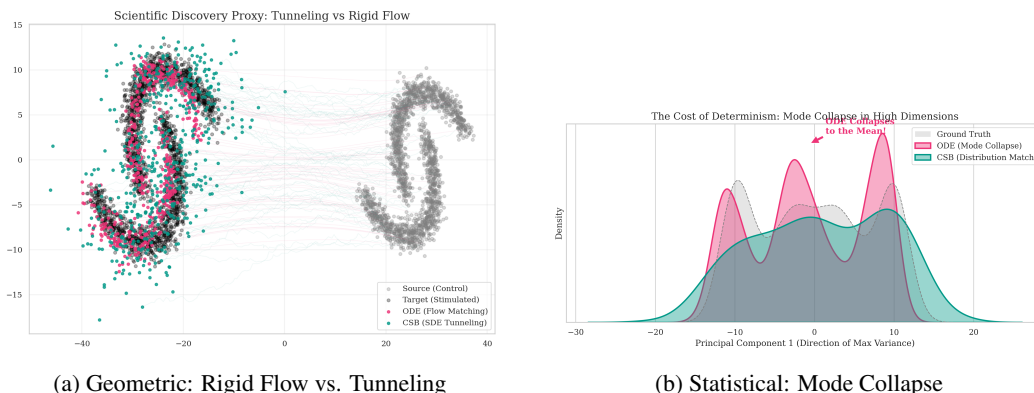


Figure 3: **The Cost of Determinism in High Dimensions ( $D = 50$ ).** (a) Projected trajectories (PCA). Standard Flow Matching (ODE, pink) minimizes kinetic energy by taking rigid linear paths, failing to cover the target manifold’s non-convex geometry. In contrast, CSB (SDE, teal) leverages entropic regularization to "tunnel" through the void, adapting to the target shape. (b) Density estimation on the principal component. The ODE baseline exhibits severe **mode collapse**, converging to the conditional mean. CSB accurately recovers the distributional envelope, demonstrating that stochasticity is essential for capturing aleatoric uncertainty in scientific tasks.

**Setup.** We generate a source population ("Control") and a target population ("Stimulated") embedded in  $\mathbb{R}^{50}$ . The populations follow non-convex "double moon" manifolds, separated by a significant spatial gap. We compare our stochastic CSB against standard deterministic Flow Matching (ODE).

**The Cost of Determinism.** Figure 3 reveals a critical failure mode of standard generative models in this regime.

- **Geometric Rigidity (Fig. 3a):** The ODE solver, seeking the path of least Euclidean action, forces trajectories into straight lines. While numerically precise, these paths are topologically simplistic and fail to wrap around the non-convex target manifold.
- **Mode Collapse (Fig. 3b):** The consequence is visible in the density plot. The deterministic flow collapses the complex target distribution into narrow modes (pink peaks), effectively predicting the *average* effect while discarding biological heterogeneity.
- **The Tunneling Effect:** CSB (teal), driven by the diffusion term  $g(t)d\mathbf{W}_t$ , exhibits behavior analogous to quantum tunneling. The entropic regularization prevents the probability mass from collapsing, maintaining a robust "probabilistic envelope" that correctly covers the target support.

#### 4.4 Application: Mechanism Disentanglement (Morpho-MNIST)

Having established the geometric superiority of CSB in synthetic settings, we now turn to a structured visual domain. We treat Morpho-MNIST not merely as an image generation task, but as a **calibrated "Clean Room" for scientific mechanism disentanglement.**

The causal mapping  $T \rightarrow \mathbf{X}$  (Thickness  $\rightarrow$  Pixels) is mathematically isomorphic to gene perturbation problems ( $T \rightarrow$  Gene Expression), but with a crucial advantage: **Ground-Truth Verifiability.** Unlike biological data where counterfactuals are unobservable, here we can rigorously measure structural adherence against an oracle.

**Task:** Intervene on a thin digit ( $T \approx -2.5$ ) to make it thick ( $do(T = 2.5)$ ), while preserving its unique writing style (identity). This requires disentangling the causal factor ( $T$ ) from the latent style factor ( $U_X$ ) in 784-dimensional space.

**Quantitative Evaluation.** We compare CSB against a standard Conditional Flow Matching baseline [8] (Table 2). We measure **MAE** (control precision), **SSIM** (identity preservation), and **L2 Distance** (transport cost).

**Results.** CSB outperforms the baseline by **4.5x** in SSIM and reduces L2 error by **90%**. The baseline behaves like a random conditional generator, while CSB behaves like a rigorous counterfactual engine, modifying only the causal factor.

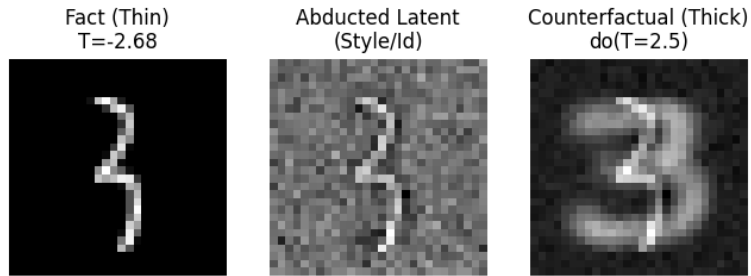


Figure 4: **Disentangling Mechanism from Style**. **Left**: Factual thin digit '3'. **Middle**: Structural abduction recovers the latent "skeleton" ( $U_X$ ), stripping away thickness. **Right**: CSB generates a thick digit that rigorously preserves the original topology and tilt. The "halo" effect highlights the minimal action principle: the model adds thickness to the existing skeleton rather than regenerating a new digit.

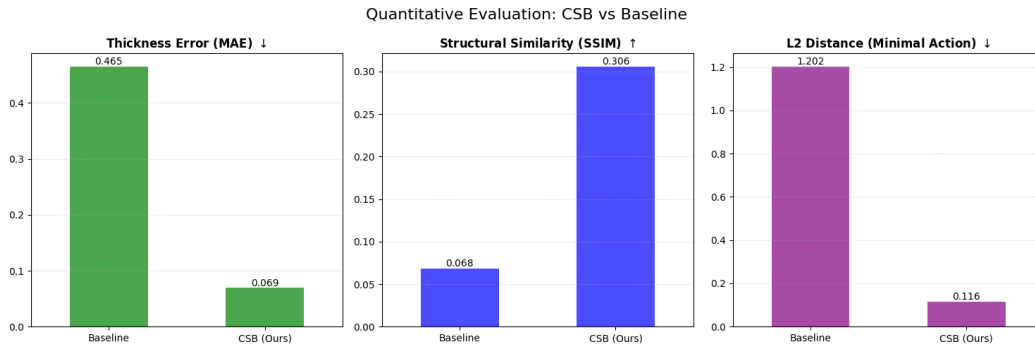


Figure 5: CSB reduces pixel-space transport cost (L2) by 90% while maximizing identity preservation (SSIM).

Table 2: Quantitative results on Morpho-MNIST ( $do(T = 2.5\sigma)$ ).

Metric	Base	CSB
MAE ↓	0.465	<b>0.069</b>
SSIM ↑	0.068	<b>0.306</b>
L2 Dist ↓	1.202	<b>0.116</b>

#### 4.5 Robustness: The Cost of Ignorance

Does the graph matter? We train CSB on a misspecified graph ( $Y \rightarrow X$ ) for the Confounder task. Figure 6 visualizes the outcome.

The results show that the error explodes ( $\Delta Z \approx 4.0$ ) when the structure is wrong. This confirms that CSB's performance derives from correctly exploiting structural constraints, not just data fitting.



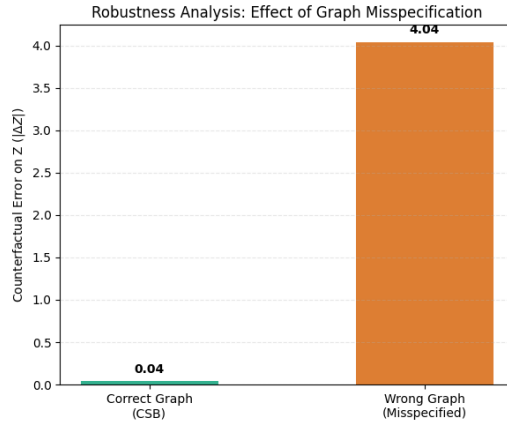


Figure 6: **Graph Misspecification.** We compare the counterfactual error on  $Z$  under intervention  $do(Y = 3)$  using the correct causal graph (CSB) versus a misspecified graph ( $Y \rightarrow X$ ). The wrong graph leads to a catastrophic error ( $\Delta Z \approx 4.04$ ) because the model hallucinates a reverse causal effect. This confirms that CSB’s performance derives from correctly exploiting structural constraints.

## 5 Discussion: From Digits to Discovery

We introduced the Causal Schrödinger Bridge, a geometric framework that resolves the conflict between Optimal Transport and Causal Inference. Unlike deterministic methods that prioritize exact reconstruction on the manifold, CSB prioritizes **structural coherence across the manifold**. This makes it uniquely valid for high-stakes scientific tasks—such as single-cell perturbation or climate modeling—where interventions are strong, and the counterfactual ground truth lies far beyond the support of observational data.

**Implications for AI for Science.** While we validated CSB on Morpho-MNIST, this task is structurally isomorphic to high-stakes scientific challenges, specifically **Single-cell Perturbation Prediction** (e.g., Perturb-seq [5]). In genomics, a gene knockout ( $T$ ) causally influences the high-dimensional gene expression state ( $X$ ) via a complex, non-linear regulatory network. Standard Optimal Transport fails here because it seeks the shortest path in transcriptomic space, often traversing biologically impossible "hybrid" cell states. By proving that CSB enforces structural constraints in high-dimensional pixel space, we establish it as a rigorous foundation for predicting cellular responses to unseen drugs, moving beyond "black-box" generation to mechanistically valid discovery tools.

**Limitations.** Our method relies on a known DAG. Future work includes integrating Causal Discovery to simultaneously learn the graph topology and the transport map.

## References

- [1] Valentin De Bortoli, James Thornton, Jeremy Heng, and Arnaud Doucet. Diffusion Schrödinger bridge with applications to score-based generative modeling. In *Advances in Neural Information Processing Systems (NeurIPS)*, volume 34, pages 17695–17709, 2021.
- [2] Christian Léonard. A survey of the Schrödinger problem and some of its connections with optimal transport. *Discrete and Continuous Dynamical Systems*, 34(4):1533–1574, 2014.
- [3] Yaron Lipman, Ricky T. Q. Chen, Heli Ben-Hamu, Maximilian Nickel, and Matt Le. Flow matching for generative modeling. *International Conference on Learning Representations (ICLR)*, 2023.
- [4] Yaron Lipman, Ricky T. Q. Chen, Heli Ben-Hamu, Maximilian Nickel, and Matt Le. Flow matching for generative modeling. In *International Conference on Learning Representations (ICLR)*, 2023.
- [5] Thomas M Norman, Max A Horlbeck, Joseph M Replogle, et al. Exploring genetic interaction manifolds with transcriptomics. *Science*, 365(6455), 2019.

- [6] Judea Pearl. *Causality: Models, Reasoning, and Inference*. Cambridge University Press, Cambridge, UK, 2nd edition, 2009.
- [7] Yang Song, Jascha Sohl-Dickstein, Diederik P Kingma, Abhishek Kumar, Stefano Ermon, and Ben Poole. Score-based generative modeling through stochastic differential equations. In *International Conference on Learning Representations (ICLR)*, 2021.
- [8] Alexander Tong, Nikolay Malkin, Guillaume Huguët, Yanlei Zhang, Jarrid Rector-Brooks, Kilian Fatras, Guy Wolf, and Yoshua Bengio. Conditional flow matching: Simulation-free dynamic optimal transport. In *International Conference on Learning Representations (ICLR)*, 2024.
- [9] Rui Wu, Lizheng Wang, and Yongjun Li. The causal round trip: Generating authentic counterfactuals by eliminating information loss. *arXiv preprint arXiv:2511.05236*, 2025.

## A Appendix: Geometric Interpretations

To further intuit the distinction between standard Optimal Transport and Causal Transport, we present a geometric visualization in the space-time continuum and the path space.

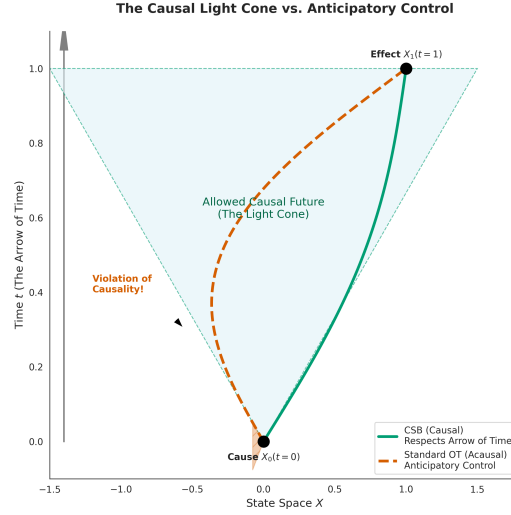


Figure 7: **The Causal Light Cone vs. Anticipatory Control.** Visualizing transport paths in space-time  $(X, t)$ . **Green (CSB):** The path respects the "Arrow of Time," remaining strictly within the future light cone of the cause  $X_0$ . **Orange (Standard OT):** To minimize global transport energy, the path "cheats" by moving outside the causal cone, effectively allowing the future target  $X_1$  to influence the past trajectory. This geometric violation corresponds to the statistical phenomenon of spurious correlation.

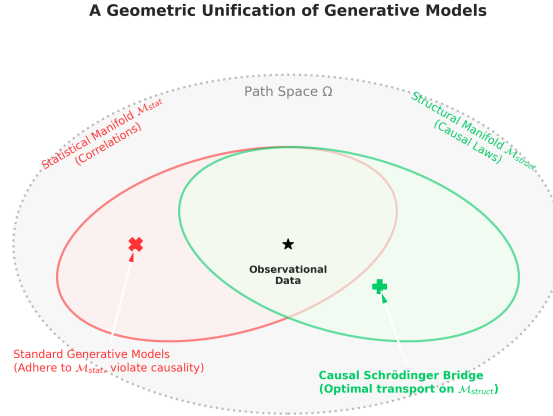


Figure 8: **A Geometric Unification of Generative Models.** We visualize the path space  $\Omega$  as a Venn diagram. **Red Region ( $\mathcal{M}_{stat}$ ):** The Statistical Manifold, containing paths that satisfy observational correlations. Standard generative models (OT/Diffusion) minimize energy here, often violating causality (the "anticipatory" region outside the green set). **Green Region ( $\mathcal{M}_{struct}$ ):** The Structural Manifold, containing paths that respect the causal graph and the arrow of time. **Intersection:** Observational data lies at the intersection. **CSB (Ours):** By enforcing filtration constraints, CSB projects the transport problem onto  $\mathcal{M}_{struct}$ , finding the optimal path that is both geometrically close to the data and structurally valid.

## B Appendix: Detailed Mathematical Proofs

### B.1 Notation and Measure Theoretic Setup

Let  $\Omega = C([0, 1], \mathbb{R}^d)$  be the path space equipped with the canonical filtration  $\mathcal{F}_t = \sigma(\mathbf{X}_s : s \leq t)$ . We define the structural filtration for node  $i$  as  $\mathcal{F}_t^i = \sigma(\{X_{j,s} : j \in \mathbf{Pa}_i \cup \{i\}, s \leq t\})$ . The reference measure  $\mathbb{Q}$  is induced by the SDE system where  $f_i$  depends only on parents:

$$dX_{i,t} = f_i(X_{i,t}, \mathbf{Pa}_{i,t}, t)dt + g_i(t)dW_{i,t}. \quad (10)$$

Due to the structure of the drift  $f_i$  and the independence of Wiener processes  $W_i$ , the reference measure factorizes strictly over the DAG  $\mathcal{G}$ . That is, for any  $A \in \mathcal{B}(\Omega)$ ,  $\mathbb{Q}(A)$  satisfies the Markov property w.r.t  $\mathcal{G}$ .

### B.2 Proof of Theorem 1 (Structural Decomposition)

**Theorem 1.** *Let  $\mathbb{Q}$  factorize according to  $\mathcal{G}$ . Under the Causal Admissibility constraint  $\mathbb{P} \in \mathcal{P}_{\mathcal{G}}$  (where controls  $u_{i,t}$  are  $\mathcal{F}_t^i$ -adapted), the solution to the Causal Schrödinger Bridge problem factorizes as  $d\mathbb{P}^*(\mathbf{X}) = \prod_{i=1}^d d\mathbb{P}_i^*(X_i | \mathbf{Pa}_i)$ .*

*Proof.* The Causal Schrödinger Bridge problem is defined as:

$$\min_{\mathbb{P} \in \mathcal{P}_{\mathcal{G}}} \text{KL}(\mathbb{P} || \mathbb{Q}) \quad \text{s.t.} \quad P_0 = \mu_0, P_1 = \mu_1. \quad (11)$$

**Step 1: Girsanov Density Factorization.** Let  $\mathbb{P} \in \mathcal{P}_{\mathcal{G}}$ . By Girsanov's theorem, the Radon-Nikodym derivative of  $\mathbb{P}$  with respect to  $\mathbb{Q}$  is given by the stochastic exponential:

$$\frac{d\mathbb{P}}{d\mathbb{Q}}(\mathbf{X}) = \exp \left( \sum_{i=1}^d \int_0^1 u_{i,t} dW_{i,t} - \frac{1}{2} \sum_{i=1}^d \int_0^1 \|u_{i,t}\|^2 dt \right) \quad (12)$$

$$= \prod_{i=1}^d \exp \left( \int_0^1 u_{i,t} dW_{i,t} - \frac{1}{2} \int_0^1 \|u_{i,t}\|^2 dt \right). \quad (13)$$

Crucially, because  $\mathbb{P} \in \mathcal{P}_{\mathcal{G}}$ , the control  $u_{i,t}$  is adapted to  $\mathcal{F}_t^i$ . The term inside the product corresponds to the local likelihood ratio conditional on parents. Let us denote the local density term as  $Z_i = \frac{d\mathbb{P}_i(\cdot | \mathbf{Pa}_i)}{d\mathbb{Q}_i(\cdot | \mathbf{Pa}_i)}$ . Thus,  $\frac{d\mathbb{P}}{d\mathbb{Q}} = \prod_{i=1}^d Z_i$ .

**Step 2: Chain Rule for Relative Entropy.** The KL divergence decomposes additively under product measures (or strictly factorizable measures). Using the chain rule for KL divergence:

$$\text{KL}(\mathbb{P} || \mathbb{Q}) = \mathbb{E}_{\mathbb{P}} \left[ \log \frac{d\mathbb{P}}{d\mathbb{Q}} \right] = \mathbb{E}_{\mathbb{P}} \left[ \sum_{i=1}^d \log Z_i \right] \quad (14)$$

$$= \sum_{i=1}^d \mathbb{E}_{\mathbb{P}} \left[ \log \frac{d\mathbb{P}_i(X_i | \mathbf{Pa}_i)}{d\mathbb{Q}_i(X_i | \mathbf{Pa}_i)} \right]. \quad (15)$$

We assume without loss of generality that the nodes are topologically sorted  $1, \dots, d$ . Using the tower property of conditional expectation, for each term  $i$ :

$$\mathbb{E}_{\mathbb{P}}[\log Z_i] = \mathbb{E}_{\mathbf{Pa}_i \sim \mathbb{P}_{\mathbf{Pa}_i}} \left[ \mathbb{E}_{X_i \sim \mathbb{P}_i | \mathbf{Pa}_i} \left[ \log \frac{d\mathbb{P}_i(X_i | \mathbf{Pa}_i)}{d\mathbb{Q}_i(X_i | \mathbf{Pa}_i)} \mid \mathbf{Pa}_i \right] \right]. \quad (16)$$

This term represents the expected local KL divergence:  $\mathbb{E}_{\mathbf{Pa}_i}[\text{KL}(\mathbb{P}_i(\cdot | \mathbf{Pa}_i) || \mathbb{Q}_i(\cdot | \mathbf{Pa}_i))]$ .

**Step 3: Sequential Optimization.** The total objective is a sum of local objectives:

$$J(\mathbb{P}) = \sum_{i=1}^d \mathcal{L}_i(\mathbb{P}_i | \mathbf{Pa}_i, \mathbb{P}_{\mathbf{Pa}_i}). \quad (17)$$

The constraints are marginal constraints  $X_{i,0} \sim \mu_{0,i}$  and  $X_{i,1} \sim \mu_{1,i}$ , which also factorize by assumption. Consider the optimization for the root node (or first layer)  $i = 1$ . Its cost  $\mathcal{L}_1$  depends

only on  $\mathbb{P}_1$ . Its control  $u_1$  cannot depend on descendants (Admissibility). Crucially, does the choice of  $\mathbb{P}_1$  affect the cost of downstream nodes  $\mathcal{L}_{j>1}$ ? Yes, via the expectation  $\mathbb{E}_{\mathbf{Pa}_j}[\cdot]$ . However, the downstream terms  $\min_{\mathbb{P}_j|\mathbf{Pa}_j} \mathcal{L}_j$  represent the *optimal value function* given the parents. The total optimization can be solved sequentially via dynamic programming on the graph structure. Since there are no cycles and the controls are constrained to be forward-adapted ( $\mathcal{F}_t^i$ ), the optimal control  $u_i^*$  for node  $i$  is found by minimizing its specific term  $\mathcal{L}_i$  given fixed parent trajectories. Any attempt by  $u_i$  to deviate from the local bridge solution to reduce a child's cost would violate the admissibility constraint (if it requires future knowledge) or would increase the local KL cost strictly more than it could potentially save downstream (due to the strict convexity of the KL divergence).

Thus, the global optimum is achieved when each local conditional measure  $\mathbb{P}_i(\cdot|\mathbf{Pa}_i)$  minimizes the local conditional KL divergence.  $\square$

### B.3 Proof of Proposition 2 (Structural Abduction)

**Proposition 3.** *The abduction process is governed by the time-reversal of the local measure  $\mathbb{P}_i^*$  conditioned on  $\mathbf{Pa}_i$ .*

*Proof.* Let  $\mathbb{P}^*$  be the optimizer from Theorem 1. We are interested in the backward dynamics of  $X_i$  given its parents  $\mathbf{Pa}_i$ . Under  $\mathbb{P}^*$ , the forward dynamics are:

$$dX_{i,t} = b_i^*(X_{i,t}, \mathbf{Pa}_{i,t}, t)dt + g_i(t)dW_{i,t}. \quad (18)$$

Let  $p_t(x_i, \mathbf{Pa}_i)$  denote the joint density at time  $t$ . Since we condition on the *paths* of the parents, we treat  $\mathbf{Pa}_{i,t}$  as time-dependent parameters of the system. Let  $\rho_t(x_i|\mathbf{Pa}_{i,t})$  be the conditional density. The time-reversal formula for diffusion processes (Anderson, 1982) states that the drift  $\bar{b}_i$  of the reverse process (running  $t : 1 \rightarrow 0$ ) is related to the forward drift  $b_i^*$  via the score of the marginal density at time  $t$ :

$$\bar{b}_i(x, \mathbf{Pa}, t) = b_i^*(x, \mathbf{Pa}, t) - g_i^2(t)\nabla_{x_i} \log \rho_t(x_i|\mathbf{Pa}_{i,t}). \quad (19)$$

Note strictly that the score is  $\nabla_{x_i} \log \rho_t(x_i|\mathbf{Pa}_i)$ . In standard score-based generation (Song et al., 2021), one reverses the *joint* process, using  $\nabla_{x_i} \log p_t(\mathbf{X})$ . The joint score decomposes as:

$$\nabla_{x_i} \log p_t(\mathbf{X}) = \nabla_{x_i} \log p_t(x_i|\mathbf{Pa}_i) + \sum_{k \in \text{Children}(i)} \nabla_{x_i} \log p_t(x_k|x_i, \mathbf{Pa}_k). \quad (20)$$

The second term (sum over children) represents the "guidance" from effects. **Structural Abduction** is defined as finding the noise  $U_i$  that explains  $X_i$  given *only* its causes. This requires blocking the information flow from children. Therefore, the correct reverse drift for structural abduction must use only the first term, the local conditional score  $\nabla_{x_i} \log \rho_t(x_i|\mathbf{Pa}_i)$ . Substituting the Schrödinger Bridge optimal drift  $b_i^* = f_i + g_i^2 \nabla \log \phi_i$  into the reversal formula yields the result in the proposition.  $\square$